Monthly Notices
of the
ROYAL ASTRONOMICAL SOCIETY

MNRAS **451,** 1795–1805 (2015) doi:10.1093/mnras/stv939

WISE colours and star formation in the host galaxies of radio-loud narrow-line Seyfert 1

A. Caccianiga,[1]★ S. Antón,[2,3] L. Ballo,[1] L. Foschini,[1] T. Maccacaro,[1] R. Della Ceca,[1] P. Severgnini,[1] M. J. Marchã,[4] S. Mateos[5] and E. Sani[6]

[1]*INAF-Osservatorio Astronomico di Brera, via Brera 28, I-20121 Milan, Italy*
[2]*Instituto de Astrofísica de Andalucía-CSIC, PO Box 3004, E-18008 Granada, Spain*
[3]*Instituto de Astrofísica e Ciências do Espaço, Universidade de Lisboa Faculdade de Ciências, Campo Grande, P-1749-016 Lisboa, Portugal*
[4]*Department of Physics and Astronomy, University College London, Gower Street, London WC1E 6BT, UK*
[5]*Instituto de Física de Cantabria (CSIC-Universidad de Cantabria), E-39005 Santander, Spain*
[6]*INAF-Osservatorio Astrofisico di Arcetri, Largo E. Fermi 5, I-50125 Firenze, Italy*

Accepted 2015 April 24. Received 2015 March 31; in original form 2015 February 17

ABSTRACT

We investigate the mid-infrared (mid-IR) properties of the largest (42 objects) sample of radio-loud narrow-line Seyfert 1 (RL NLS1) collected to date, using data from the *Wide-field Infrared Survey Explorer*. We analyse the mid-IR colours of these objects and compare them to what is expected from different combinations of AGN and galaxy templates. We find that, in general, the host galaxy emission gives an important contribution to the observed mid-IR flux in particular at the longest wavelengths (*W*3, at 12 μm, and *W*4, at 22 μm). In about half of the sources (22 objects), we observe a very red mid-IR colour ($W4 - W3 > 2.5$) that can be explained only using a starburst galaxy template (M82). Using the 22 μm luminosities, corrected for the AGN contribution, we have then estimated the star formation rate (SFR) for 20 of these 'red' RL NLS1, finding values ranging from 10 to 500 $M_{\odot}$ yr^{-1}. For the RL NLS1 showing bluer colours, instead, we cannot exclude the presence of a star-forming (SF) host galaxy although, on average, we expect a lower SFR. Studying the radio (1.4 GHz) to mid-IR (22 μm) flux ratios of the RL NLS1 in the sample, we found that in ∼10 objects the SF activity could represent the most important component also at radio frequencies, in addition (or in alternative) to the relativistic jet. We conclude that both the mid-IR and the radio emission of RL NLS1 are a mixture of different components, including the relativistic jet, the dusty torus and an intense SF activity.

Key words: galaxies: active – galaxies: jets – galaxies: nuclei – galaxies: starburst.

1 INTRODUCTION

The importance of the nuclear active accretion phase (AGN) in the context of galaxy evolution has been fully recognized only in the last years (e.g. see Heckman & Best 2014 for a recent review). According to the galaxy–AGN co-evolution scenario, at high redshifts, both star-forming (SF) activity and nuclear accretion must have proceeded simultaneously and at high rates thanks to the abundance of cold gas and to the frequent galaxy mergers that made the gas available for both processes. In a second phase, when the AGN luminosity was high enough to expel the gas from the galaxy, both star formation and accretion rate gradually reduced eventually leading to a 'passive' elliptical hosting a quiescent super-massive black hole (SMBH).

At low redshift, however, galaxy interactions and/or internal galaxy dynamics can destabilize the residual gas and make it available for new episodes of SF and nuclear activity at high accretion rates. Mathur (2000) has proposed that the so-called narrow-line Seyfert 1 (NLS1) galaxies, a peculiar sub-class of AGN that is characterized by rapidly accreting central black holes with relatively small masses (between 10^5 and 10^8 $M_{\odot}$), may represent the low-redshift, low-luminosity analogues of the first high-z quasars, hosted by rejuvenated, gas-rich galaxies. In support to this hypothesis, it has been noted that NLS1 are more frequently associated to host galaxies with large levels of SF activity than broad-line Seyfert 1 (BLS1) galaxies (e.g. Deo, Crenshaw & Kraemer 2006; Sani et al. 2010, 2012). In this context, NLS1 could be systems that are building up mass, evolving eventually into BLS1. The time-scale of this

★ E-mail: alessandro.caccianiga@brera.inaf.it

process should depend on the radiative efficiency of the accretion process, as discussed in Orban de Xivry et al. (2011).

Interestingly, NLS1 may be considered as 'young systems' also from the radio point of view. NLS1s are typically radio-quiet (RQ) sources with only a small fraction that can be classified as radio loud (RL, ∼7 per cent, Komossa et al. 2006 and about 50 in total known to date, Foschini 2011). The radio properties of these RL NLS1 seem to be different from those observed in RL BLS1 mainly because of the lack of extended radio structures, except for very few cases (e.g. Doi et al. 2012). It has been proposed that at least some of the RL NLS1 can be associated to young radiogalaxies whose relativistic jet is still digging its way through the interstellar medium (ISM) of the host galaxy possibly evolving into a 'classical' giant radiogalaxy (Moran 2000; Oshlack, Webster & Whiting 2001; Gallo et al. 2006; Komossa et al. 2006; Yuan et al. 2008; Caccianiga et al. 2014). Notably, young and compact radiogalaxies are observed also in the three RL quasi-stellar objects (QSO) discovered to date at $z \sim 6$ (Frey et al. 2011, 2012). This further increases the possible analogies between local NLS1 and high-z QSO.

The possibility that NLS1 are 'young' systems where the AGN–galaxy co-evolution is taking place and where, in some cases, a young relativistic jet is ejected and observed in the early phase of its evolution, is intriguing: the study of these sources may offer a unique opportunity of investigating the co-evolution mechanism in both RL and RQ objects at relatively low redshifts where the observational constraints are less challenging with respect to high-z QSO.

In this paper, we focus on the RL fraction of NLS1 that is still poorly studied. In particular, we want to assess if RL NLS1 are similar to RQ NLS1 for what concerns their preference in being hosted by SF galaxies. To date, only few RL NLS1 have been studied from this point of view. Optical imaging has revealed the existence of arms or circumnuclear rings (possibly the consequence of a recent merger) and the presence of a circumnuclear starburst in at least one RL NLS1 (1H 0323+342; Zhou et al. 2007; Antón, Browne & Marchã 2008; León-Tavares et al. 2014). In a recent paper (Caccianiga et al. 2014), a new case of RL NLS1 has been presented whose spectral energy distribution (SED) is strongly suggestive of the presence of a quite intense star formation (∼50 $M_\odot$ yr^{-1}). The presence of this intense SF was revealed by the mid-infrared (mid-IR) data at 12 and 22 μm from the *Wide-field Infrared Survey Explorer* (*WISE*) catalogue (Wright et al. 2010) that showed a clear excess with respect to a typical dust emission from an RQ AGN or to the IR non-thermal spectrum coming from a jet. We now want to extend such a result on a large sample of RL NLS1 to establish whether the presence of star formation is a peculiar characteristic of some isolated sources or, instead, is a global property of the entire class.

The sample and the data used in this study are presented in Section 2. In Section 3, we discuss how the mid-IR colours (particularly those including the 22 μm band) of the sources cannot be satisfactorily explained by the AGN emission alone. In Section 4, we consider the effect of galaxy emission on the observed IR colours and we infer the presence of an SF host in many objects of the sample. In Section 5, we compare the 1.4 GHz to 22 μm flux ratios of the RL NLS1 with those of blazars and infrared galaxies while in Section 6 we estimate the star formation rate (SFR) present in the sources with the reddest $W3 - W4$ colours. Conclusions are finally presented in Section 7.

Throughout the paper, we assume a flat Λ cold dark matter cosmology with $H_0 = 71$ km s^{-1} Mpc^{-1}, $\Omega_\Lambda = 0.7$ and $\Omega_M = 0.3$. Spectral indices are defined assuming $S_\nu \propto \nu^{-\alpha}$.

2 THE SAMPLE OF RL NLS1 AND *WISE* DATA

Foschini et al. (2015) have presented an extended study of the 42 RL NLS1 with a large radio-loudness parameter[1] (>10; see Foschini et al. 2015 for details) and a flat radio spectrum (i.e. with blazar-like characteristics) discovered so far.[2] Several pieces of information, from the radio to the X-ray and gamma-ray band, have been collected and studied. The physical properties of the inner SMBH, like its mass and the accretion rate, have been also discussed. This is the largest sample of RL NLS1 collected so far and, therefore, it represents the best starting point to study the incidence of star formation in the galaxies hosting these AGNs. It should be noted, however, that the type of selection of this sample, namely the requirement of a flat radio spectrum, strongly favours the presence of a relativistically beamed jet emission (as in blazars), which could be important also in the mid-IR band. This may partly (or totally) hide the emission from the host galaxy. To date, however, only few RL NLS1 without 'blazar-like' characteristics have been discovered and, therefore, the Foschini et al. (2015) sample is the only possibility for this type of analysis, at the moment.

The mid-IR data have been collected from the *WISE* All-Sky catalogue (Wright et al. 2010) and, in particular, we have used the last version of the catalogue, the AllWISE data release (November 2013), which has an enhanced photometric sensitivity and accuracy compared to the 2012 *WISE* All-Sky Data Release. All the NLS1 of the sample are detected [signal-to-noise ratio (S/N) > 3] in the *WISE* survey at 3.4 and 4.6 μm (*W*1 and *W*2 bands, respectively), all but one are detected at 12 μm (*W*3) and 37 are detected at 22 μm (*W*4). Data for the 42 RL NLS1 are reported in Table 1.

Four sources are flagged in the catalogue as possibly extended, i.e. the source profile fit has a large (>3) χ^2 value in one or more bands. In one of these sources (J0324+3410/1H 0323+342) imaging in R and B has revealed the existence of extended structures (arms/rings) that could be the consequence of a recent merger (Antón et al. 2008). In the remaining three sources, the available optical images [from the Sloan Digital Sky Survey (SDSS) or the United Kingdom Schmidt Telescope (UKST)] show the presence of a nearby (<5 arcsec) object, possibly in interaction with the NLS1. Finally, three sources in the catalogue (J0324+3410, J0849+5108 and J0948+0022) are flagged as variable in the *W*1 and *W*2 band and for two of them (J0849+5108 and J0948+0022) intra-day variability has been studied by Jiang et al. (2012).

In Fig. 1, we show the distribution of the *WISE* colours in the *W*1, *W*2 and *W*3 filters for the 41 RL NLS1 detected in all the three bands. In this figure, we also show some characteristic regions recently adopted to select different types of AGN (see figure caption for details). Not surprisingly, all the objects fulfil the AGN definition ($W1 - W2 > 0.8$) proposed by Stern et al. (2012) and all but two lie in the AGN wedge discussed by Mateos et al. (2012, 2013). Most (78 per cent) of the RL NLS1 occupy the region where blazars are usually found (blue and green solid regions) while nine sources lie outside it. One source, in particular, shows a very blue

[1] The radio-loudness parameter used in Foschini et al. (2015) is defined as the 5 GHz to 4400Å flux density ratio.

[2] We note that only 22 sources out of 42 have a measured radio spectral index. Of these 22 objects, 20 have a flat slope ($\alpha_R \leq 0.5$) while 2 have α_R marginally above this value (0.55 and 0.58, respectively) but consistent with it taking into account the errors (see Foschini et al. 2015 and also Richards & Lister 2015 for the recently measured spectral index of J0953+2836). The remaining 20 sources have no information on the radio spectral index and should be considered more properly as 'flat-spectrum candidates'.

Table 1. *WISE* data on the sample of RL NLS1.

Name	Other name	z	*W*1 (3.4 μm)			*W*2 (4.6 μm)			*W*3 (12 μm)			*W*4 (22 μm)		
			mag	unc.	S/N	mag	unc.	S/N	mag	unc.	S/N	mag	unc.	S/N
J0100−0200	FBQSJ0100−0200	0.227	12.859	0.023	46.5	11.754	0.023	46.7	8.407	0.024	44.7	6.187	0.060	18.0
J0134−4258	PMNJ0134−4258	0.237	12.157	0.024	46.1	11.129	0.021	52.4	8.125	0.022	49.1	5.924	0.042	25.9
J0324+3410	1H 0323+342 03 [a, b]	0.061	10.743	0.022	49.1	9.791	0.020	54.7	7.179	0.016	67.4	4.847	0.027	40.1
J0706+3901	FBQSJ0706+3901	0.086	12.888	0.024	45.6	11.959	0.022	48.9	8.599	0.026	41.0	6.049	0.051	21.4
J0713+3820	FBQSJ0713+3820	0.123	10.040	0.022	49.3	8.990	0.020	53.5	6.261	0.015	74.8	3.984	0.021	51.7
J0744+5149	NVSSJ074402+514917	0.460	13.397	0.024	44.4	12.384	0.025	43.7	9.636	0.044	24.7	6.829	0.069	15.6
J0804+3853	SDSSJ080409.23+385348.8	0.211	11.745	0.023	46.4	10.750	0.020	54.3	8.077	0.022	48.8	5.372	0.032	33.5
J0814+5609	SDSSJ081432.11+560956.6	0.509	14.221	0.027	40.4	13.139	0.028	38.9	10.411	0.074	14.6	n.d.	–	–
J0849+5108	SDSSJ084957.97+510829.0 [a,b]	0.584	12.887	0.024	44.7	11.956	0.022	48.8	10.042	0.049	22.0	7.552	0.135	8.0
J0902+0443	SDSSJ090227.16+044309.5	0.532	13.927	0.026	41.0	13.096	0.029	37.7	10.015	0.064	16.9	7.058	0.086	12.7
J0937+3615	SDSSJ093703.02+361537.1	0.179	12.165	0.024	45.7	11.202	0.021	51.5	8.135	0.021	50.8	5.472	0.035	31.1
J0945+1915	SDSSJ094529.23+191548.8	0.284	12.042	0.024	45.9	11.078	0.022	50.1	8.279	0.023	47.4	5.705	0.044	25.0
J0948+0022	SDSSJ094857.31+002225.4 [b]	0.585	13.282	0.024	44.5	12.204	0.023	46.5	9.096	0.032	33.4	6.682	0.088	12.3
J0953+2836	SDSSJ095317.09+283601.5	0.658	14.809	0.032	33.9	13.924	0.039	27.6	11.335	0.179	6.1	n.d.	–	–
J1031+4234	SDSSJ103123.73+423439.3	0.376	14.323	0.029	37.8	13.300	0.030	35.8	10.446	0.078	14.0	8.392	0.343	3.2
J1037+0036	SDSSJ103727.45+003635.6	0.595	15.108	0.037	29.5	13.854	0.039	27.8	10.698	0.103	10.6	n.d.	–	–
J1038+4227	SDSSJ103859.58+422742.2	0.220	12.549	0.024	46.0	11.532	0.021	50.7	8.870	0.028	39.1	6.576	0.058	18.8
J1047+4725	SDSSJ104732.68+472532.0	0.798	14.749	0.031	35.2	13.641	0.033	33.3	10.435	0.089	12.2	7.748	0.189	5.7
J1048+2222	SDSSJ104816.58+222239.0	0.330	13.499	0.025	44.3	12.356	0.026	42.4	9.292	0.044	24.5	7.087	0.114	9.5
J1102+2239	SDSSJ110223.38+223920.7	0.453	13.167	0.024	45.7	12.042	0.024	44.7	9.146	0.034	31.5	6.489	0.069	15.7
J1110+3653	SDSSJ111005.03+365336.3	0.630	16.038	0.058	18.6	15.230	0.090	12.1	n.d.	–	–	n.d.	–	–
J1138+3653	SDSSJ113824.54+365327.1	0.356	14.055	0.026	42.1	13.139	0.028	39.1	10.532	0.084	13.0	8.007	0.207	5.2
J1146+3236	SDSSJ114654.28+323652.3	0.465	14.099	0.027	39.8	13.208	0.029	38.0	10.509	0.080	13.6	8.571	0.313	3.5
J1159+2838	SDSSJ115917.32+283814.5	0.210	13.451	0.025	42.6	12.343	0.023	46.3	9.015	0.034	32.2	5.982	0.042	25.8
J1227+3214	SDSSJ122749.14+321458.9	0.137	11.441	0.023	48.2	10.328	0.020	53.7	7.420	0.018	60.8	4.802	0.024	44.8
J1238+3942	SDSSJ123852.12+394227.8	0.623	15.327	0.037	29.7	14.525	0.050	21.9	11.700	0.183	5.9	n.d.	–	–
J1246+0238	SDSSJ124634.65+023809.0	0.363	14.163	0.029	37.4	13.094	0.029	37.2	10.346	0.084	12.9	7.517	0.161	6.7
J1333+4141	SDSSJ133345.47+414127.7	0.225	13.102	0.023	47.2	11.947	0.022	49.5	8.763	0.024	44.6	5.846	0.043	25.1
J1346+3121	SDSSJ134634.97+312133.7	0.246	13.744	0.025	43.1	12.850	0.026	41.8	9.693	0.039	27.6	7.283	0.105	10.3
J1348+2622	SDSSJ134834.28+262205.9	0.918	14.710	0.029	37.0	13.368	0.028	38.2	10.400	0.064	16.9	8.574	0.287	3.8
J1358+2658	SDSSJ135845.38+265808.5	0.331	13.133	0.024	44.7	12.069	0.022	48.3	9.225	0.030	36.2	6.531	0.058	18.6
J1421+2824	SDSSJ142114.05+282452.8	0.538	13.674	0.025	43.0	12.607	0.024	45.8	9.614	0.038	28.7	7.194	0.096	11.3
J1505+0326	SDSSJ150506.47+032630.8	0.409	14.028	0.027	40.1	13.093	0.029	37.8	9.840	0.045	24.4	7.061	0.086	12.7
J1548+3511	SDSSJ154817.92+351128.0	0.479	13.770	0.026	42.1	12.771	0.024	44.8	9.883	0.035	31.4	7.200	0.072	15.1
J1612+4219	SDSSJ161259.83+421940.3	0.234	13.308	0.024	45.8	12.199	0.022	48.9	8.135	0.018	62.0	5.572	0.030	36.3
J1629+4007	SDSSJ162901.30+400759.9	0.272	13.290	0.024	45.6	12.177	0.022	49.1	9.471	0.037	29.4	6.865	0.070	15.6
J1633+4718	SDSSJ163323.58+471858.9 [a]	0.116	12.135	0.023	46.6	11.318	0.020	53.2	7.642	0.017	64.0	4.974	0.024	44.8
J1634+4809	SDSSJ163401.94+480940.2	0.495	14.883	0.028	39.0	13.884	0.031	35.1	10.711	0.049	22.1	8.081	0.119	9.2
J1644+2619	SDSSJ164442.53+261913.2	0.145	13.283	0.024	44.7	12.294	0.024	44.4	9.455	0.040	27.1	7.019	0.100	10.8
J1709+2348	SDSSJ170907.80+234837.7	0.254	13.758	0.026	42.5	12.785	0.024	44.4	9.903	0.044	24.6	7.343	0.117	9.2
J2007−4434	PKS 2004−447	0.240	13.445	0.025	43.7	12.349	0.024	44.8	9.467	0.035	31.1	7.025	0.098	11.0
J2021−2235	IRAS 20181−2244 [a]	0.185	11.880	0.023	48.0	10.997	0.021	51.6	7.601	0.017	63.5	4.710	0.034	32.2

Notes. [a]Flagged as extended in one or more bands in the AllWISE catalogue (ext_flg=3 or 5). [b]Flagged as possibly variable in *W*1 and *W*2 band in the AllWISE catalogue (var_flg>7).

*W*2 − *W*3 colour (*W*2 − *W*3 = 1.914), which is significantly different from the values observed in the other objects. This source, however, is one of the three objects flagged as variable (J0849+5108, one of the sources detected also in gamma-rays by *FERMI*; Foschini et al. 2015). Indeed, the *W*1 and *W*2 magnitudes reported in Jiang et al. (2012), based on the previous version of the *WISE* All-Sky catalogue, are significantly fainter ($\Delta \sim 1.1$ mag) than the ones reported here. Therefore, the position on the *W*1 − *W*2 versus *W*2 − *W*3 plot of this objects is likely affected by the observed flux variations and, for this reason, it is not indicative of the real spectral distribution of the source.[3]

3 AGN EMISSION AND *WISE* COLOURS

Even if the RL NLS1 are broadly clustered around the region expected for a power-law (PL) spectrum (with a spectral index α_{IR} ranging from ∼0.5 to ∼1.5), many departures from this region are also observed: some sources occupy the region above this line (towards redder *W*1 − *W*2 colours) while others occupy a region bluer in *W*1 − *W*2 and redder in *W*2 − *W*3.

If the *WISE* emission of these RL NLS1 were totally dominated by the non-thermal jet, we would expect a PL or a broken PL spectral shape. In Fig. 2 (left), we show the region on the *W*1 − *W*2 versus

[3] It should be considered that the AllWISE catalogue, that we are using in this work, has been produced by combining all the data from both the *WISE* cryogenic and post-cryogenic survey phases, the latter being carried out only in the *W*1 and *W*2 bands. Therefore, the periods over which the images have been collected and combined are different for the four bands.

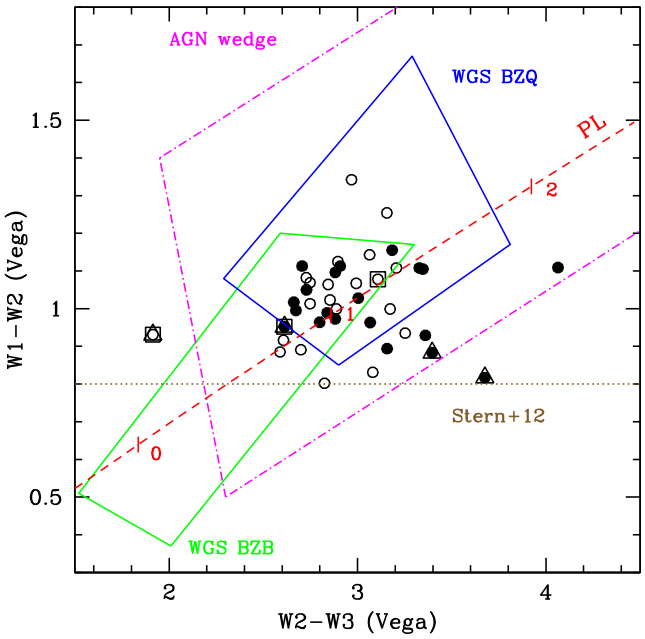

Figure 1 The *WISE* colours of the RL NLS1 in the Foschini et al. (2015) sample. Open and filled circles indicate the RL NLS1 with a redshift above and below 0.3, respectively. Sources circled by an open square are flagged as variable in the AllWISE catalogue while sources circled by triangles are flagged as extended. Different characteristic regions used to select AGNs are also plotted: the blazar 'WISE Gamma-ray Strip' (WGS) for BL Lacs and FSRQ (BZB and BZQ, respectively, solid lines), as defined by Massaro et al. (2012), the AGN wedge (dot–dashed line) as defined by Mateos et al. (2012) and Mateos et al. (2013) for X-ray-selected AGNs, the mid-IR criterion ($W1 - W2 > 0.8$, brown dotted line) proposed by Stern et al. (2012). Finally, the red dashed line indicates the region covered by a simple power-law spectrum (slopes of $\alpha = 0$, 1 and 2 are indicated by tidemarks).

$W2 - W3$ plot where we expect to find a source whose IR spectrum is described by a broken PL with a slope before the break ranging from 0.5 to 1 and a slope after the break of 1.5 and with the position of the break varying within the *WISE* bands (dark blue shaded area). As clear from Fig. 2 (left), we expect that a source with a broken PL spectrum would fall above the PL line. Several sources are actually found in this region although the majority of them seem to be much 'redder', in terms of $W1 - W2$ colour, than what is expected from a broken PL.

In principle, a significant level of extinction could change the position of a source with a PL spectrum moving it away from the expected region, towards redder values of $W1 - W2$ and $W2 - W3$. However, since these sources are, by definition, type 1 AGNs, i.e. objects where both the AGN continuum and the broad emission lines are visible in the optical spectrum, the extinction is not expected to have an important impact on the mid-IR colours (e.g. see Mateos et al. 2015). In the upper-right side of both panels of Fig. 2, we indicate with an arrow the expected effect of an extinction of $A_V = 2$ mag at the mean redshift of the sample ($\langle z \rangle = 0.36$). An A_V of 2 mag is the maximum expected for type 1 AGNs as discussed, for instance, in Caccianiga et al. (2008).

It is also possible that part (or the totality) of the observed IR emission is produced by the RQ component of the source (i.e. the dusty torus) and not by the non-thermal jet. Indeed, the presence of this component is expected and it has been revealed in many RL AGN and blazars (e.g. Malmrose et al. 2011; Raiteri et al. 2014; Gurkan, Hardcastle & Jarvis 2014; Castignani & De Zotti 2015). In Fig. 2 (left), we plot the position of three RQ type 1 QSO templates[4] (from Polletta et al. 2007) in the range of redshift between 0 and 0.9 (the range of z of the sample, red solid lines). The regions occupied by these three templates lie above the PL line and reach redder $W1 - W2$ values than the broken PL, in particular for high-redshift sources (z between 0.5 and 0.9). Notably, the source with the reddest value of $W1 - W2$ (=1.34, J1348+2622) is also the object with the largest redshift in the sample ($z = 0.918$). Only the TQSO1 template can reach such a red $W1 - W2$ colour that a broken PL, instead, does not seem able to reproduce. We consider this as an indication that, at least in a number of objects, the mid-IR emission is probably mainly produced by the RQ component (i.e. the torus) rather than the relativistic jet.

Finally, we consider also the possibility that both the dusty-torus and the jet emissions are present in the spectrum. To this end, we combine the three QSO templates with a PL emission, at different values of redshift (from 0 to 0.9), varying the relative normalizations of the two components (light blue shaded area).

From the analysis of Fig. 2 (left), we conclude that the sources lying above the PL line in the $W1 - W2$ versus $W2 - W3$ plot could be explained either by a broken PL emission, expected when the jet emission is dominant, or by an RQ AGN (i.e. torus) emission or by a combination of the two components. Only one object (J0849+5108) lies above the PL but in a isolated region towards blue $W2 - W3$ values ($W1 - W2 = 0.931$ and $W2 - W3 = 1.914$). As said before, this is a highly variable source and, therefore, its position is not indicative of the actual IR spectral shape.

In ∼10 cases, the objects fall well below the PL line and, therefore, their colours are not easily explained by a torus/jet emission nor by a combination of the two. The number of sources not explained by these models is even higher if we consider the longest wavelength magnitude ($W4$, at $\lambda = 22\,\mu$m) in the diagnostic plot, i.e. if we plot $W1 - W2$ versus $W3 - W4$ (Fig. 2, right). As before, we overplot the expected regions followed by a PL, a broken PL and an RQ AGN component plus a PL emission. From this figure, it is clear that only few objects can be explained by these models while the large majority (∼80–90 per cent) lie well below the PL line thus requiring a different (very red) component. As described in the following section, the best candidate for the emission of this red component is the host galaxy.

4 THE EFFECT OF GALAXY DILUTION ON IR COLOURS

We consider here the effect of the combination of an AGN plus the host galaxy emission on the *WISE* colour plots. To this end, we use some representative templates of the Spitzer-Space-Telescope Wide-area Infrared Extragalactic Survey (SWIRE) library (Polletta et al. 2007). Specifically, we use an early-type galaxy ('Ell5' template), an Sc galaxy ('Sc' template) and a starburst galaxy ('M82' template, Fig. 3). We start from a galaxy template and add a PL with different slopes and varying the relative AGN/galaxy normalization.

[4] These templates have been derived by Polletta et al. (2007) by combining the SDSS quasar composite spectrum and rest-frame IR data of a sample of optically selected type 1 QSOs observed in the SWIRE program. The three templates have the same optical spectrum but three different IR SEDs: a mean IR spectrum, obtained from the average fluxes of all measurements ('QSO1'), a template with high IR/optical flux ratio template, obtained from the highest 25 per cent measurements per bin ('TQSO1'), and a low-IR emission SED obtained from the lowest 25 per cent measurements per bin ('BQSO1').

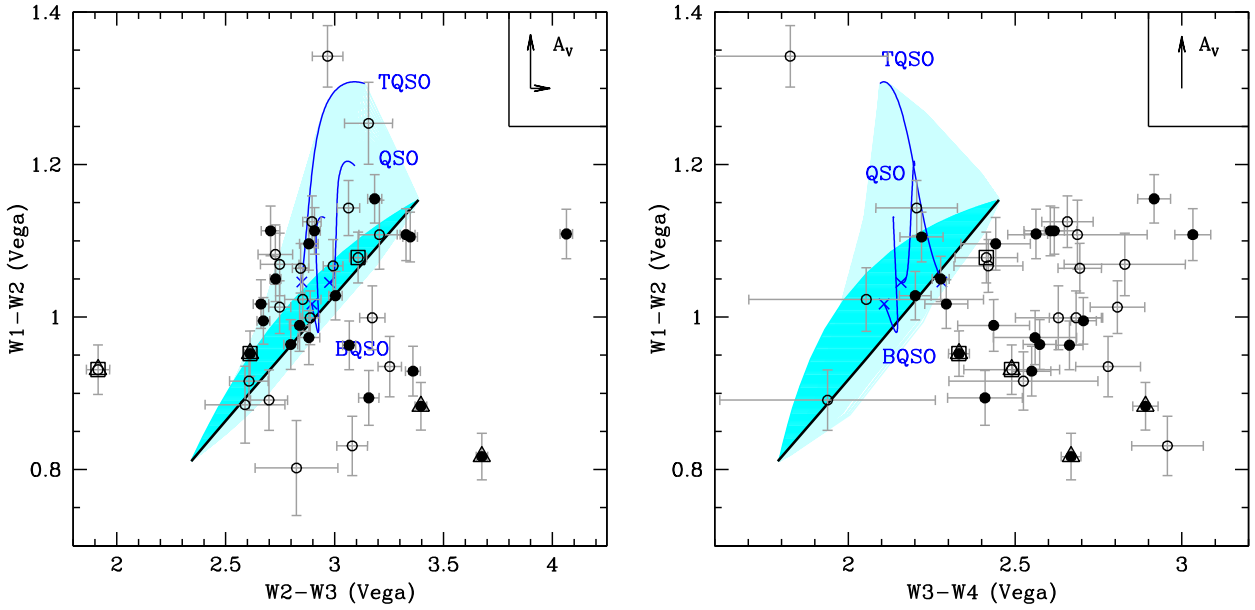

Figure 2. The expected positions on the $W1 - W2$ versus $W2 - W3$ (left) and $W1 - W2$ versus $W3 - W4$ (right) plot of AGNs with different shapes of IR spectrum: (1) a simple power law (PL; black thick line) with slope ranging from 0.5 to 1.5; (2) a smooth broken PL, with slope before the break ranging from 0.5 to 1 and a slope of 1.5 after the break and with the break position varying within the *WISE* bands (dark blue shaded area); (3) an RQ AGN emission described by the three QSO templates from the SWIRE library (blue lines labelled as QSO, BQSO and TQSO, see text for a description and Polletta et al. 2007 for more details) and with a redshift ranging from 0 (indicated by a cross) to 0.9 (the maximum value of the sample); (4) a combination of RQ AGN emission plus a PL spectrum (light blue shaded area). In particular, we show the result of all the different combinations of slopes (from 0.5 to 1.5), redshift (from 0 to 0.9) and relative RQ AGN to PL normalization. The arrows in the upper-right corners show the expected effect of an extinction of $A_V = 2$ mag at the mean redshift of the sample. An $A_V = 2$ mag is the maximum value expected for type 1 AGNs. We do not plot the arrow along the $W3 - W4$ since the extinction has a negligible effect in this case. Points as in Fig. 1.

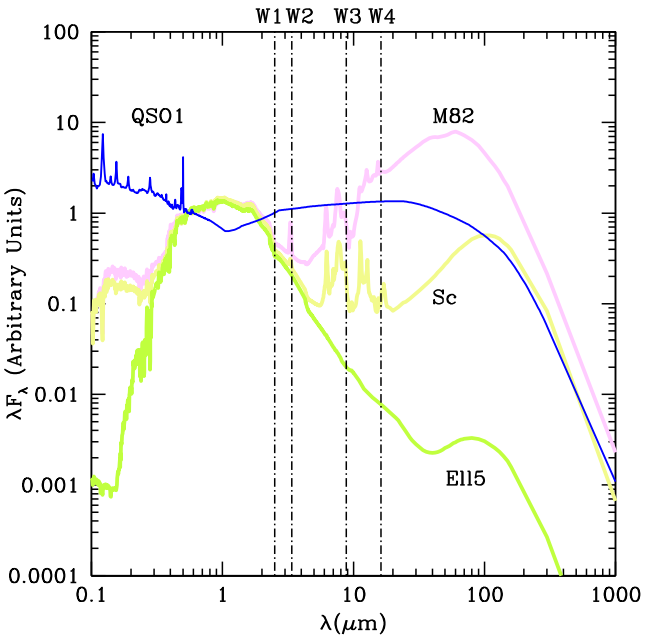

Figure 3. Templates from the SWIRE library (Polletta et al. 2007) used in the analysis. On the top axis we indicate the centres of the four *WISE* bands at the average redshift of the sample (0.36).

In Fig. 4, we show the predicted effect of the host galaxy dilution on a PL emission. An early-type host is expected to move the AGN colours towards the left/bottom side of the plot, i.e. it is expected to produce bluer colours in both $W1 - W2$ and $W2 - W3$ ($W3 - W4$) values as it gets more and more important. A starburst host, instead, is expected to make the $W1 - W2$ values bluer than the PL while both the $W2 - W3$ and the $W3 - W4$ colours become redder, thus bringing the object on the right-most side of the plot. Other starburst templates show a similar behaviour. This is the effect of the strong IR emission of the starburst component that becomes more and more important in the $W3$ (and $W4$) bands.

In Fig. 4, we also show the position of SDSSJ143244.91+301435.3, an RL NLS1 discussed in Caccianiga et al. (2014) whose SED has revealed the presence of an SF host galaxy with an SFR of 50 $M_\odot$ yr^{-1}. In order to correctly reproduce the infrared SED (in particular the $W4$ photometric point) of this object, we used the M82 template by Polletta et al. (2007).

Fig. 4 (left) shows that the host galaxy may be contributing significantly to the mid-IR emission in a number (10) of sources of the sample, i.e. those objects that occupy the region below the PL line. For the sources just below this line, the contribution from the host galaxy in these *WISE* bands is not enough to distinguish the type of the host galaxy. In ∼4 cases, instead, the very red $W2 - W3$ colours seem to favour an SF host galaxy. We note that the position of SDSSJ143244.91+301435.3 on this plot does not clearly indicate an SF host galaxy. Indeed, as discussed in Caccianiga et al. (2014), the strongest indication for an M82-like host galaxy comes from the $W4$ band (22 μm), which shows a clear excess. Fig. 4 (right) shows that using the $W4$ filter we can better discriminate between the different types of host galaxy. In particular, the mid-IR colours of the 22 sources with $W3 - W4 > 2.5$ (like SDSSJ143244.91+301435.3) can be explained only by combining the AGN emission to a starburst galaxy host.

In order to better show the effect of the host galaxy on the observed spectrum, we report in Fig. 5 the average UV-to-mid-IR SED of the NLS1 of the sample divided according to the value of

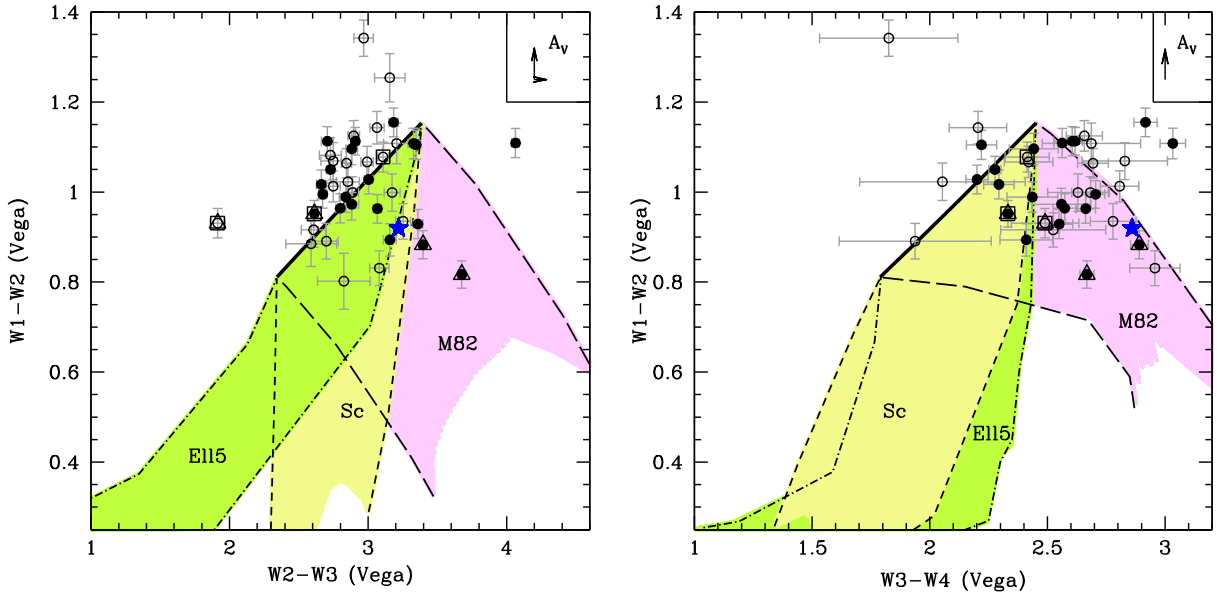

Figure 4. The effect of the host galaxy emission on a power-law (PL) spectrum, in the *WISE* colours plots ($W1 - W2$ versus $W2 - W3$, left, and versus $W3 - W4$, right). The three regions between the long-dashed/short-dashed/point-dashed lines represent the expected paths of a combination of PL plus a galaxy template taken from the SWIRE library (M82, Sc and Ell5, respectively; Polletta et al. 2007), varying the relative intensity of the two components, the PL slopes (ranging from 0.5 to 1.5) and the redshift of the source ($\pm 1\sigma = \pm 0.2$ from the mean value of z). Note that the limits are different from those of Fig. 2 in order to better show the different paths produced by different host galaxies. Symbols and arrows as in Fig. 2. The blue star indicates the position of SDSSJ143244.91+301435.3, an RL NLS1 studied in detail by Caccianiga et al. (2014) and whose SED is suggestive of the presence of a starburst host galaxy.

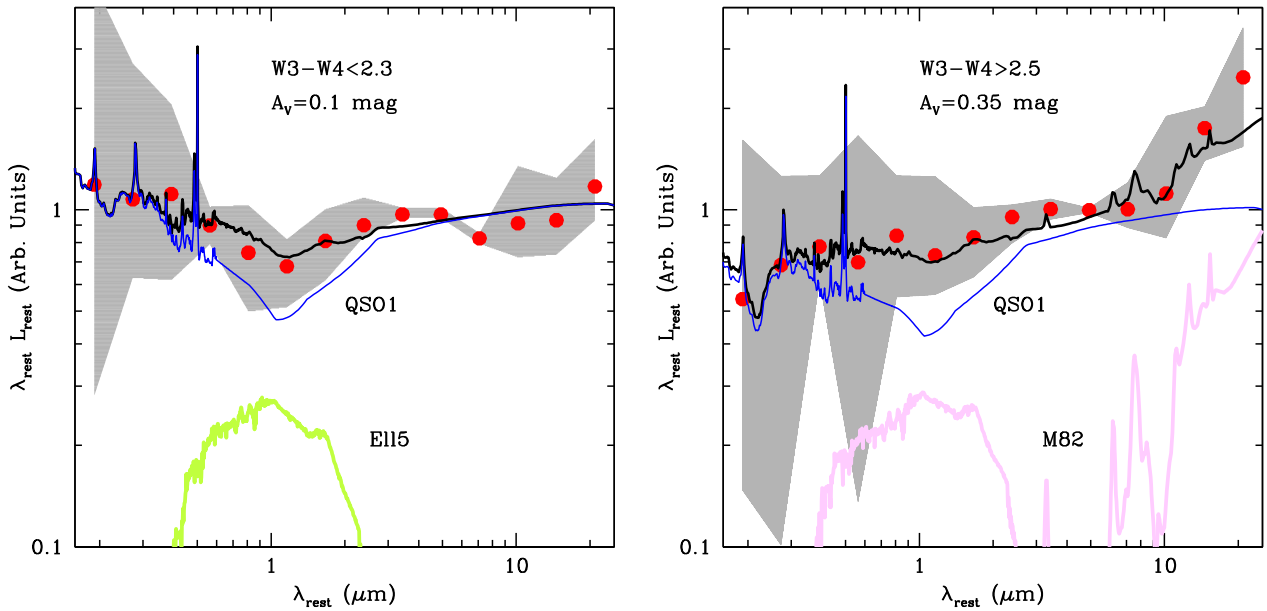

Figure 5. Average UV-to-mid-IR SED of the RL NLS1 in the sample divided according to the $W3-W4$ colour. Red points represent the average values of $\log\lambda L_\lambda$ in each bin of $\log\lambda$ while the shaded area represents the region including 68 per cent of points. The thick black line is a model composed by a reddened (the A_V value is indicated in the label) AGN template (QSO1 from Polletta et al. 2007) plus a galaxy template: in the left-hand panel an early-type galaxy template (Ell5) is used while, in the right-hand panel, we adopt a starburst galaxy template (M82).

$W3 - W4$ colour (greater than 2.5 or lower than 2.3, in order to keep more separated the two groups). The average SEDs have been created by normalizing each rest-frame SEDs at 4 μm and computing the average value of $\log\lambda L_\lambda$ in bins of $\log\lambda$. The grey area reports the region including 68 per cent of points. The data used to produce these SED are taken from Foschini et al. (2015) and include, besides *WISE* photometry, data from *Swift*-Ultraviolet/Optical Telescope (UVOT) observations and from existing public surveys like SDSS (DR9, Ahn et al. 2012), 2MASS (Cutri et al. 2003) and USNO-B (Monet et al. 2003).

To correctly interpret the shape of these average SEDs, we model them with the sum of a galaxy and a QSO template, varying the relative normalization, the amount of nuclear extinction and the host morphology (see Ballo et al. 2014 for a more detailed description of the procedure). We consider different combinations of extinctions and galaxy/AGN templates and we find that templates with a low-IR

emission (early-type/Sc galaxies) are able to describe the observed average SED of the objects with bluer $W3-W4$ colours (left-hand panel) while these templates systematically fail in reproducing the $W3/W4$ data points in the average SED of sources with redder $W3-W4$ (right-hand panel). In this latter case, instead, a starburst galaxy template, like M82, is more suited to reproduce the steep increase of the data points towards longer wavelengths.

We note that the two average SEDs show some differences also in the UV/optical part. We can explain this difference with a different (average) extinction level. While to model the average SED of the sources with a blue $W3-W4$ colour we have to apply only a small level of extinction ($A_V = 0.1$ mag), in the case of the red $W3-W4$ objects, we need a higher value of A_V (0.35 mag). The explanation of this result could be related to the enhanced presence of dust in highly SF galaxies with respect to less SF galaxies (see e.g. Buat et al. 2002; Domínguez et al. 2013).

5 JET OR STAR FORMATION?

So far, we have focused our analysis on the UV-to-mid-IR data and, in particular, on the mid-IR colours. From these data, we have inferred the presence of an SF/starburst host galaxy in at least half of the RL NLS1 in the sample. Since an intense SF is expected to produce an important emission also in the radio band it is possible that the radio luminosities observed in these sources are in part contaminated by the SF activity. In principle, it is even possible that a high SFR can explain the totality of the observed radio emission. This would be an unexpected result, since the sample under investigation is composed by objects with large radio-loudness parameters and, in some cases, a flat radio spectrum. These properties are usually considered as strong indications that the radio emission is likely produced by a relativistic jet pointing towards the observer (and, thus, relativistically beamed).

Since jet-dominated objects and SF galaxies have significantly different radio-to-mid-IR flux ratios, it is interesting to compare this parameter computed for the RL NLS1 to the values usually observed in jet-dominated AGN (i.e. blazars), from the one hand, and to the values observed in SF galaxies, on the other hand.

To quantify the radio-to-mid-IR flux ratios, we use two equivalent parameters. The two-point spectral-index, defined between 1.4 GHz and 22 μm (rest frame[5]) as

$$\alpha_{1.4}^{22} = -\frac{\log\left(S_{1.4\ \mathrm{GHz}}/S_{22\,\mu\mathrm{m}}\right)}{\log\left(\nu_{1.4\ \mathrm{GHz}}/\nu_{22\,\mu\mathrm{m}}\right)} \quad (1)$$

which is typically used in blazars studies, and the parameter $q22$ defined as:

$$q22 = \log\left(S_{22\,\mu\mathrm{m}}/S_{1.4\ \mathrm{GHz}}\right). \quad (2)$$

The radio-to-mid-IR indices for the 37 RL NLS1 in the sample detected in the $W4$ band are reported in Fig. 6. For comparison, we also report the distribution of $\alpha_{1.4}^{22}$ for a sample of 430 blazars with a quasar spectrum (flat-spectrum radio quasar, FSRQ) extracted from the BZCAT (Massaro et al. 2009) and detected with high significance (S/N>10) in all the *WISE* filters. To help the comparison, this latter histogram has been re-normalized by a factor 10. We also indicate the typical range of radio-to-mid-IR values observed in the infrared galaxies reported by Rieke et al. (2009). In particular, we report the observed range of $q24$, a quantity similar to $q22$ but defined at 24 μm instead of 22 μm using Multiband Imaging Photometer for *Spitzer* (MIPS) data. The average value found is 1.2–1.4, depending on the infrared luminosity of the source, with a dispersion of 0.24 dex.

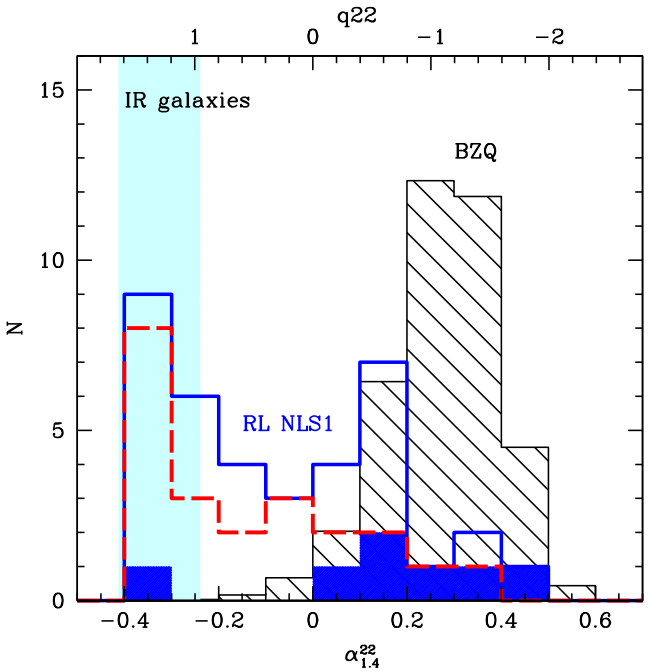

Figure 6. Distribution of the two-point spectral index between radio (1.4 GHz, rest frame) and mid-IR (22 μm, rest frame) of the RL NLS1 (blue histogram) and of blazars (BZQ) in the BZCAT (black shaded histogram). This latter histogram has been re-scaled by a factor 10 to facilitate the comparison. The flux densities have been *K*-corrected assuming a slope of 0 in the radio and using the observed IR slope between 12 and 22 μm. The filled blue histogram shows the RL NLS1 detected in the gamma-ray by *FERMI*. The dashed red histogram includes only the red ($W3-W4>2.5$) objects. The top axis reports the values of $q22$. For comparison, the typical range of $q24$ (defined at 24 μm instead of 22 μm) observed in the infrared galaxies is also indicated (light blue region; Rieke et al. 2009).

The first consideration on Fig. 6 is that the RL NLS1 span a wide interval of radio-to-mid-IR indices, covering the entire range between the values observed in infrared galaxies to those observed in blazars. This is a first evidence that the radio and mid-IR emission of these sources are a mixture of different components. In sources with steep $\alpha_{1.4}^{22}$ indices (>0.2), i.e. within the range of values observed in blazars, the relativistic jet is likely the dominant component in the radio band (while in the mid-IR different emission could be present, including the dusty torus and/or the host galaxy). In sources with $\alpha_{1.4}^{22} < -0.25$ (i.e. $q22>1$) the SF activity may be contributing significantly to the observed radio emission. This is likely true, for instance, in the sources with red $W3-W4$ colours (dashed red histogram), that are the majority in this interval of $q22$ values. The most obvious interpretation for the objects showing intermediate values, instead, is a combination of jet and SF (plus the dusty torus, in the mid-IR).

In support to the hypothesis that the relativistic jet is dominant in sources with steep $\alpha_{1.4}^{22}$ values we note that 6 out of the 15 RL NLS1 with $\alpha_{1.4}^{22}>0$ (i.e. 40 per cent) are detected in gamma-rays by *FERMI* (filled histogram in Fig. 6), something that is usually considered as an indication for the presence (and the dominance) of a relativistic jet, while only one object (J1102+2239) out 22 with $\alpha_{1.4}^{22}<0$ (5 per cent) is a *FERMI* source. The dominance of the

[5] For the *K*-correction we use, for each source, the slope computed between 12 and 22 μm (observed frame) fluxes and we assume $\alpha = 0$ in the radio band.

relativistic jet in four of the *FERMI* detected RL NLS1 with $q22 > 0$ (J0324+3410, J0849+5108, J0948+0022 and J1505+0326) has been recently quantified also by Angelakis et al. (2015) by means of a systematic monitoring in the radio and millimetric bands.

This confirms the presence and the importance of the relativistic jet in the sources with a positive value of $\alpha_{1.4}^{22}$ while it seems to suggest that other mechanisms are at work in addition (or instead of) to the relativistic jet in most of the remaining sources. It is worth noting, however, that a low value of $\alpha_{1.4}^{22}$ (or a high value of $q22$) does not necessarily exclude the presence of a jet as demonstrated by the detection in gamma-rays by *FERMI* of one of the objects with a high value of $q22$ (=1.34, J1102+2239)[6]. Another example is the sources J1227+3214 that, in spite of a large $q22$ value (=1.29), has an inverted radio spectrum ($\alpha_R = -1.04$; Foschini et al. 2015) something that suggests a non-thermal origin of the radio emission (or at least of a fraction of it). It should be considered that variability can play an important role in determining the properties of a source at different wavelengths, including its position within the histogram of Fig. 6: during high activity periods, a source may appear as jet dominated in many (if not all) frequencies, showing for instance a flat radio spectrum, a strong gamma-ray emission or a high radio-to-mid-IR flux ratio, while, during low activity periods, the signs for the presence of the jet can be hidden by the RQ AGN emission or even by the host galaxy light. For all these reasons, simultaneous multiwavelengths monitoring campaigns, together with radio follow-ups, in particular at Very-long-baseline interferometry (VLBI) resolution, are fundamental to disentangle the different components and establish their relative importance at different wavelengths.

6 ESTIMATE OF THE STAR FORMATION RATE

In this section we want to quantify the intensity of the star formation at least in those sources where the mid-IR colours are suggestive of the presence of a starburst host. Specifically, we consider here only the 22 sources with a red $W3 - W4$ colour ($W3 - W4 > 2.5$). To limit the contamination due to the AGN nucleus (either the dusty torus or the jet component) we analyse here the longest wavelength *WISE* band (*W*4 at 22 μm) since, according to the results previously discussed, this is the band where the SF nature of the host galaxy seems to emerge more clearly.

We first compute the 22 μm luminosities (λL_λ). We derive the 22 μm flux densities from the *W*4 magnitudes[7] and applied a *K*-correction using the spectral slope computed between 12 and 22 μm (observed frame) fluxes. The computed 22 μm luminosities of the sources range between 10^{10} and 10^{12} $L_\odot$ with a large fraction (76 per cent) of objects with $L_{22\,\mu m} > 10^{11}$ $L_\odot$.

In order to derive an estimate of the SFR in these sources, we can use the relation presented in Rieke et al. (2009) between SFR and $L_{24\,\mu m}$ (their equation 10 and equation 11). However, since the $L_{22\,\mu m}$ luminosity is likely contaminated by the AGN, in particular the dusty-torus component, we have to apply a correction. To estimate the importance of the AGN emission at 22 μm, we proceed as follows.

Jet contribution. We estimate the contribution from the jet starting from the radio flux density measured at 1.4 GHz, assuming the average value of the $\alpha_{1.4}^{22}$ observed in the blazars (FSRQ) of the BZCAT catalogue ($\alpha_{1.4}^{22} = 0.27$, see Fig. 6) and subtract it from the observed flux density at 22 μm (rest frame). For the two objects that have $\alpha_{1.4}^{22} > 0.27$ the estimate of 22 μm due to the galaxy is not possible and we exclude them from the analysis. For the sources with radio-to-mid-IR flux ratios similar to those observed in IR galaxies ($\alpha_{1.4}^{22} < -0.25$), the correction for the jet emission is negligible (<1 per cent) and has no impact on the final results. As discussed in the previous section, in these sources even the radio emission could be mainly (or totally) attributed to the star formation activity.

Torus contribution. We estimate the contribution from the torus using the flux densities at 4.6 μm (rest frame[8]) and assuming that this is entirely produced by the AGN (jet and torus). This is a reasonable assumption since, as discussed in the previous sections, in the *W*1 and *W*2 filters we are probably preferentially observing the AGN emission (see also the average SEDs of Fig. 5). This is also consistent with what has been recently found by Mateos et al. (2015) studying the mid-IR properties of a sample of X-ray-selected AGN. If also the host galaxy is contributing to the 4.6 μm emission then the final estimate of the 22 μm emission from the host galaxy, and hence of the SFR, would be even higher. As for the 22 μm flux density, also the 4.6 μm flux density has been corrected for the jet contribution, using the average 1.4 GHz to 4.6 μm spectral index observed in the FSRQ of the BZCAT ($\langle\alpha_{1.4}^{4.6}\rangle = 0.43$). Using the resulting flux density and the slope between 4.6 and 22 μm measured on the QSO1 template from SWIRE ($\alpha = 1.1$), we can then estimate the contribution of the torus at 22 μm and subtract also this component from the observed flux density.

We find that the average contribution from the torus at 22 μm is more important (∼40 per cent) than that from the jet (∼7 per cent). In order to take into account the uncertainties related to the initial assumption on the $\alpha_{1.4}^{22}$ of the jet and the IR slope of the torus, we have repeated these computations with different input values: $\alpha_{1.4}^{22} = 0.15$ and 0.39 (i.e. the 1σ interval observed in the FSRQ of the BZCAT) and $\alpha_{IR} = 1.0$–1.1, for the infrared slope of the torus, corresponding to the extreme values measured in the three QSO1 template of SWIRE (TQSO1, BQSO1 and QSO1). We take the extreme values obtained in all these combinations as the uncertainty interval of the 22 μm luminosity from the host galaxy. The computed 22 μm luminosities of the host galaxies range from 10^{10} to 5×10^{11} $L_\odot$.

We then use the 22 μm luminosity corrected for the AGN contribution to estimate the SFR using the relation presented in Rieke et al. (2009), their equation 10 and equation 11, and assuming $L_{24\,\mu m}(\mathrm{MIPS}) \sim L_{22\,\mu m}$. The results are reported in Table 2 and plotted in Fig. 7. The SFR of these 20 objects are above ∼10 $M_\odot$ yr^{-1} and, in several cases, larger than 100 $M_\odot$ yr^{-1}, similarly to what is usually observed in luminous infrared galaxies (LIRGs) or even in ultraluminous infrared galaxies (ULIRGs; Sanders & Mirabel 1996). This result confirms and quantifies what we have inferred from the analysis of the mid-IR colours, i.e. the presence of an intense SF activity in at least half of the RL NLS1 in sample.

We finally note that an SFR estimate for the RL NLS1 with $W3 - W4 < 2.5$ would not be reliable since the evidence of a significant contribution of an SF host galaxy to the emission at 22 μm is not

[6] Interestingly, this source was indicated by Foschini et al. (2015) as possible outlier in the gamma-ray/radio correlation.

[7] For this conversion, we assume an IR spectral slope of 1. The differences in the derived flux densities when assuming significantly different slopes, from −1 to 2, are below 0.7 per cent

[8] For the *K*-correction we use here, for each source, the observed slope computed between 3.4 and 4.6 μm.

Table 2. Estimates of the star formation rate for the sources with $W3 - W4 > 2.5$ and with $\alpha_{1.4}^{22} < 0.27$, based on the 22 μm luminosities corrected for the AGN contribution (see text for details). Column 1: source name; column 2: logarithm of the SFR derived from the 22 μm luminosity; column 3: uncertainty interval on the SFR that takes into account only the errors on the estimate of the 22 μm luminosities of the host galaxies (see text for a description). In addition to this uncertainty it should be considered also the one related to the SFR–L(24 μm) relation (about ∼0.2 dex; Rieke et al. 2009); column 4: logarithm of the 22 μm to 1.4GHz flux density ratio; column 5: $W1 - W2$ colour; column 6: $W3 - W4$ colour; column 7: radio spectral slope ($S_\nu \propto \nu^{-\alpha}$) from Foschini et al. (2015).

Name	log SFR ($M_\odot$ yr^{-1})	log SFR unc. ($M_\odot$ yr^{-1})	$q22$	$W1 - W2$	$W3 - W4$	α_R
(1)	(2)	(3)	(4)	(5)	(6)	(7)
J0706+3901	0.95	[0.92, 0.98]	0.82	0.93	2.55	–
J0744+5149	2.50	[2.43, 2.56]	0.47	1.01	2.81	–
J0804+3853	1.95	[1.94, 1.96]	1.48	0.99	2.70	–
J0902+0443	2.70	[1.70, 3.70]	−0.65	0.83	2.96	0.07 ± 0.01
J0937+3615	1.92	[1.91, 1.93]	1.31	0.96	2.66	–
J0945+1915	2.14	[2.06, 2.21]	0.60	0.96	2.57	–
J1102+2239	2.48	[2.47, 2.49]	1.34	1.13	2.66	–
J1138+3653	1.16	[0.16, 2.16]	−0.15	0.92	2.52	0.5 ± 0.09
J1159+2838	2.11	[2.10, 2.11]	1.39	1.11	3.03	–
J1227+3214	1.73	[1.71, 1.74]	1.29	1.11	2.62	−1.04 ± 0.07
J1246+0238	1.83	[0.83, 2.83]	−0.36	1.07	2.83	0.55 ± 0.06
J1333+4141	2.17	[2.16, 2.17]	1.39	1.16	2.92	–
J1358+2658	2.11	[2.09, 2.12]	1.30	1.06	2.69	–
J1548+3511	2.18	[1.18, 3.18]	−0.77	1.00	2.68	0.26 ± 0.01
J1612+4219	2.35	[2.35, 2.36]	1.32	1.11	2.56	–
J1629+4007	1.39	[1.06, 1.72]	0.29	1.11	2.61	−0.68 ± 0.02
J1633+4718	1.83	[1.74, 1.92]	0.23	0.82	2.67	0.42 ± 0.01
J1634+4809	2.07	[1.93, 2.20]	0.15	1.00	2.63	–
J1709+2348	1.36	[1.33, 1.39]	0.96	0.97	2.56	–
J2021−2235	2.48	[2.46, 2.50]	0.81	0.88	2.89	0.5 ± 0.07

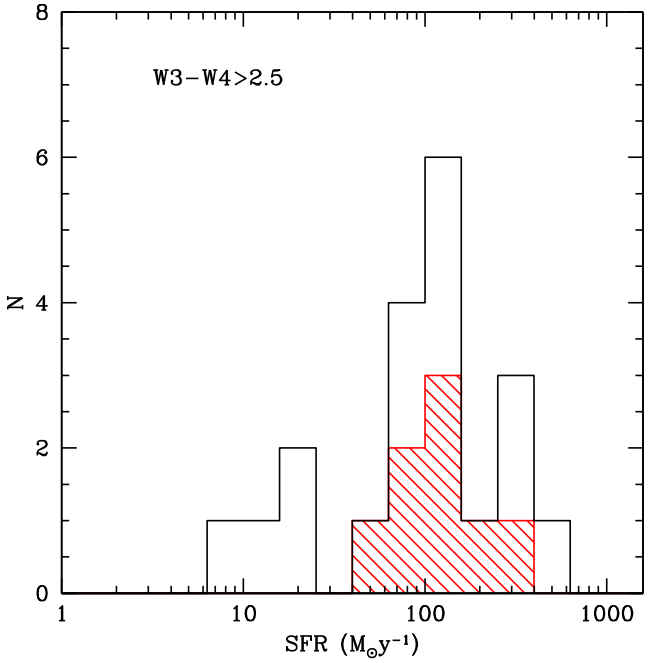

Figure 7. Star formation rate estimated from the 22 μm luminosity corrected for the AGN contribution (see text for details). This estimate has been done for the objects whose *WISE* colours suggest the presence of a star-forming host galaxy ($W3 - W4 > 2.5$). Shaded histogram includes only the sources with a $q22 > 1$.

clear. Running the analysis described above on the blue objects, we find that, on average, only a small fraction (∼8 per cent) of the observed 22 μm luminosities can be due to the host galaxy the remaining fraction being produced by the torus (56 per cent) and by the jet (36 per cent). The estimate of the 22 μm luminosity due to the host galaxy (and therefore the SFR quantification) depends too critically on the starting assumptions on the $\alpha_{1.4}^{22}$ of the jet and on the IR spectral shape of the dusty torus to give reliable results. The only stable quantities that we can derive are the upper limits on the SFR based on the total observed 22 μm luminosities. These values do not exclude the presence of an intense SFR ($> 10\,M_\odot$ yr^{-1}) also in the objects with $W3 - W4 < 2.5$. From these upper limits alone, it is not possible to understand whether the host galaxies of these AGNs are intrinsically different from those observed in 'red' RL NLS1 or, rather, their SF activity is simply hidden by a particularly strong nuclear light. We have, however, other pieces of information that can help to distinguish between these two hypotheses.

In Fig. 5, we have presented the average SEDs of red ($W3 - W4 > 2.5$) and blue ($W3 - W4 < 2.3$) objects, that clearly show different shapes at $\lambda > 10$ μm. While the average SED of the red objects requires the presence of an M82-like template to be correctly reproduced, the average SED of the blue objects can be modelled using an Sc or Ell5 template. An M82 template would overpredict the emission at $\lambda > 10$ μm. We note that the normalization of the host galaxy template is quite well constrained in the spectral region around ∼1 μm (rest frame). This suggests that the blue objects are hosted, on average, by different types of host galaxy.

In order to assess whether there are differences also in the luminosities of the AGN (either the RQ or the jet component) between red and blue objects we can compare the average luminosities at

4 μm, where the torus emission is expected to dominate, and in the radio band. At 4 μm the average values are only marginally different, with the blue objects being about 30 per cent more luminous than the red ones. Even in the radio band we do not have evidence that the jets in the blue objects are more luminous than the jets present in the red sources. Rather, the average 1.4 GHz power of blue objects is a factor ∼1.6 fainter than in red objects. The average 22 μm luminosity, instead, is significantly different between the two groups of sources, where the red objects are almost a factor 2 more luminous that the blue sources.

Overall, these numbers seem to indicate that the lack of a clear detection of the host galaxy in the blue objects is not due to a more luminous radio jet and/or AGN (RQ) but, rather, to a less luminous 22 μm emission, i.e. a less important SF component at work in these sources. As explained above, the upper limits on the SFR are in any case large so we cannot exclude the presence of an intense SF also in these sources but, on average, their activity, if present, seems to be less intense than the one observed in the host galaxies of the red RL NLS1. This picture needs a confirmation through an accurate follow-up (in particular of the blue RL NLS1) in the mid-IR or in the far-IR spectral region, where the maximum output of the SF activity is expected.

7 CONCLUSIONS

We have analysed the mid-IR colours of a sample of 42 RL NLS1 using *WISE* data with the aim of quantifying, for the first time, the SF activity in the galaxies hosting this class of AGNs. The sources cover the redshift interval from 0.06 to 0.92. Thirty-seven objects are detected in all the four *WISE* bands. In order to understand the origin of the mid-IR emission in these sources we have compared their positions on different diagnostic plots with those expected from a combination of AGN and host galaxy templates. The results can be summarized as follows:

(i) In general, the RL NLS1 of the sample occupy a region in the $W1 - W2$ versus $W2 - W3$ plot (commonly used in the literature) that is typical of emission line AGN, both RQ and RL.

(ii) *WISE* colours can be reproduced by a combination of AGN and host galaxy emission, the relative importance of the two components depending strongly on the band under consideration. While the emission from 3.4 up to 12 μm (observed frame) of most (3/4) of the sources can be explained by the AGN alone (either the relativistic jet, the dusty torus or a combination of the two), at 22 μm the emission usually requires the (red) contribution from the host galaxy.

(iii) Twenty-two sources show very red $W3 - W4$ colours (>2.5) that can be explained only by assuming the presence of a young and 'active' host galaxy, i.e. a starburst galaxy similar to M82. In the remaining cases, the intensity of the AGN emission in the mid-IR bands does not allow to unambiguously assess the type of host galaxy.

(iv) The 22 μm luminosities of the NLS1 detected in $W4$ are typically above 10^{11} $L_{\odot}$. We have used these luminosities, corrected for the AGN contribution, to estimate the SFR for 20 out of the 22 sources with $W3 - W4 > 2.5$. The computed values of SFR range between 10 and 500 $M_{\odot}$ yr^{-1}. These values are similar to those observed in LIRG or even in ULIRG (Sanders & Mirabel 1996). For the sources with $W3 - W4 < 2.5$ the presence of an SF host galaxy cannot be excluded although the SFR is expected to be, on average, lower than in red sources.

(v) Although the sample studied here has been designed to include NLS1 with a relativistic jet (possibly pointing towards Earth), by means of a selection of sources with a large radio-loudness parameter (radio-loudness parameter >10) and, preferentially, a flat radio spectrum ($\alpha_R < 0.5$; see Foschini et al. 2015 for details), our analysis shows that in the mid-IR the jet is not necessarily the dominant component, even in sources that have been detected in gamma-rays by *FERMI*. In particular, we have estimated that, on average, at 22 μm only ∼20 per cent of the luminosity of the sources with $W3 - W4 > 2.5$ comes from the jet, the remaining part being emitted by the dusty torus and by the host galaxy.

(vi) Even at radio frequencies (1.4 GHz) the emission of a number (∼10) of sources in the sample, i.e. those with high mid-IR-to-radio luminosity ratios, is not necessarily due to the jet but it is likely produced, in part or entirely, by the SF activity.

In conclusion, our analysis has shown that RL NLS1 are often associated to 'active' host-galaxies, with SFR in the typical range of LIRG/ULIRG sources. Therefore, from this point of view, RL NLS1 are more similar to RQ NLS1 than to RL AGNs with broader emission lines, usually hosted by 'passive' elliptical galaxies. These results support the idea that NLS1, both RQ and RL, are systems in the early phase of their evolution, when the host galaxy is experiencing a high level of SF activity and, at the same time, the central SMBH is rapidly accreting and building up mass. Studying the properties of these sources and their differences with respect to the other RL AGNs will help us to understand the role of relativistic jets in the AGN/galaxy evolution and to unveil any possible form of feedback (either positive or negative). To this end, simultaneous follow-ups, both in the mid-IR and in the radio, are mandatory in order to accurately disentangle the different components at work in these active nuclei and to study their possible interplay.

ACKNOWLEDGEMENTS

We thank the referee for useful comments that improved the paper. This publication makes use of data products from the *Wide-field Infrared Survey Explorer*, which is a joint project of the University of California, Los Angeles, and the Jet Propulsion Laboratory/California Institute of Technology, funded by the National Aeronautics and Space Administration. Part of this work was supported by the COST Action MP0905 'Black Holes in a Violent Universe' and by the European Commission Seventh Framework Programme (FP7/2007-2013) under grant agreement no. 267251 Astronomy Fellowships in Italy (AstroFIt). The authors acknowledge financial support from the Italian Ministry of Education, Universities and Research (PRIN2010-2011, grant no. 2010NHBSBE). Support from the Italian Space Agency is acknowledged by LB (contract ASI INAF NuSTAR I/037/12/0). SM acknowledges funding from the Spanish Ministry of Economy and Competitiveness under grant AYA2012-31447, which is partly funded by the FEDER programme. SM acknowledges financial support from the ARCHES project (7th Framework of the European Union, no. 313146).

REFERENCES

Ahn C. P. et al., 2012, ApJS, 203, 21
Angelakis E. et al., 2015, A&A, 575, 55
Antón S., Browne I. W. A., Marchã M. J., 2008, A&A, 490, 583
Ballo L., Severgnini P., Della Ceca R., Caccianiga A., Vignali C., Carrera F. J., Corral A., Mateos S., 2014, MNRAS, 444, 2580
Buat V., Boselli A., Gavazzi G., Bonfanti C., 2002, A&A, 383, 801

Caccianiga A. et al., 2008, A&A, 477, 735
Caccianiga A. et al., 2014, MNRAS, 441, 172
Castignani G., De Zotti G., 2015, A&A, 573, 125
Cutri R. M. et al., 2003, The IRSA 2MASS All-Sky Point Source Catalog, NASA/IPAC, Pasadena, CA
Deo R. P., Crenshaw D. M., Kraemer S. B., 2006, AJ, 132, 321
Doi A., Nagira H., Kawakatu N., Kino M., Nagai H., Asada K., 2012, ApJ, 760, 41
Domínguez A. et al., 2013, ApJ, 763, 145
Foschini L., 2011, in Foschini L., Colpi M., Gallo L., Grupe D., Komossa S., Leighly K., Mathur S. eds, Proc. Narrow-Line Seyfert 1 Galaxies and their place in the Universe, PoS, Trieste, Italy, p. 24
Foschini L. et al., 2015, A&A, 575, A13
Frey S., Paragi Z., Gurvits L. I., Gabányi K. E., Cseh D., 2011, A&A, 531, L5
Frey S., Gurvits L. I., Paragi Z., Gabanyi K., 2012, in Proc. Resolving The Sky - Radio Interferometry: Past, Present and Future, PoS, Trieste, Italy, PoS(RTS2012)041
Gallo L. C. et al., 2006, MNRAS, 370, 245
Gurkan G., Hardcastle M. J., Jarvis M. J., 2014, MNRAS, 438, 1149
Heckman T. M., Best P. N., 2014, ARA&A, 52, 75
Jiang N. et al., 2012, ApJ, 759, L31
Komossa S., Voges W., Xu D., Mathur S., Adorf H.-M., Lemson G., Duschl W. J., Grupe D., 2006, AJ, 132, 531
León-Tavares J. et al., 2014, ApJ, 795, 58
Malmrose M. P., Marscher A. P., Jorstad S. G., Nikutta R., Elitzur M., 2011, MNRAS, 732, 116
Massaro E., Giommi P., Leto C., Marchegiani P., Maselli A., Perri M., Piranomonte S., Sclavi S., 2009, A&A, 495, 691
Massaro F., D'Abrusco R., Tosti G., Ajello M., Gasparrini D., Grindlay J. E., Smith H. A., 2012, ApJ, 750, 138
Mateos S. et al., 2012, MNRAS, 426, 3271
Mateos S., Alonso-Herrero A., Carrera F., Blain A., Severgnini P., Caccianiga A., Ruiz A., 2013, MNRAS, 434, 941
Mateos S. et al., 2015, MNRAS, 449, 1422
Mathur S., 2000, MNRAS, 314, L17
Monet D. G. et al., 2003, AJ, 125, 984
Moran E. C., 2000, New Astron. Rev., 44, 527
Orban de Xivry G., Davies R., Schartmann M., Komossa S., Marconi A., Hicks E., Engel H., Tacconi L., 2011, MNRAS, 417, 2721
Oshlack A. Y. K. N., Webster R. L., Whiting M. T., 2001, ApJ, 558, 578
Polletta M. et al., 2007, ApJ, 663, 81
Raiteri C. M. et al., 2014, MNRAS, 442, 629
Richards J. L., Lister M. L., 2015, ApJ, 800, L8
Rieke G. H., Alonso-Herrero A., Weiner B. J., Pérez-González P. G., Blaylock M., Donley J. L., Marcillac D., 2009, ApJ, 692, 556
Sanders D. B., Mirabel I. F., 1996, ARA&A, 34, 749
Sani E., Lutz D., Risaliti G., Netzer H., Gallo L. C., Trakhtenbrot B., Sturm E., Boller T., 2010, MNRAS, 403, 1246
Sani E. et al., 2012, MNRAS, 424, 1963
Stern D. et al., 2012, ApJ, 753, 30
Wright E. L. et al., 2010, AJ, 140, 1868
Yuan W., Zhou H. Y., Komossa S., Dong X. B., Wang T. G., Lu H. L., Bai J. M., 2008, ApJ, 685, 801
Zhou H. et al., 2007, ApJ, 658, L13

This paper has been typeset from a TEX/LATEX file prepared by the author.